Bulletin of Mathematical Biology, Vol. 59, No. 2, pp. 295–323, 1997
Elsevier Science Inc.

0092-8240/97 $17.00 + 0.00

S0092-8240(96)00073-0

THE HYDROMECHANICS OF HYDROCEPHALUS: STEADY-STATE SOLUTIONS FOR CYLINDRICAL GEOMETRY

■ MARIUSZ KACZMAREK[1]
Department of Civil and Environmental Engineering,
Duke University,
Durham, NC 27708, U.S.A.
(*E.mail: mkk@hum.amu.edu.pl*)

■ RAVI P. SUBRAMANIAM[2]
Division of Neurosurgery,
Robert Wood Johnson Medical School,
Suite 411, Three Cooper Plaza,
Camden, NJ 08103, U.S.A.
(*E.mail: ravi@ciit.org*)

■ SAMUEL R. NEFF
Neurosurgery,
Wills Eye Hospital,
900 Walnut Street,
Philadelphia, PA 19107, U.S.A.

Hydrocephalus is a state in which the circulation of cerebrospinal fluid is disturbed. This fluid, produced within the brain at a constant rate, moves through internal cavities in it (ventricles), then exits through passages so that it may be absorbed by the surrounding membranes (meninges). Failure of fluid to move properly through these passages results in the distention of the passages and the ventricles. Ultimately, this distention causes large displacements and distortion of brain tissue as well as an increase of fluid in the extracellular space of the brain (edema). We use a two-phase model of fluid-saturated material to simulate the steady state of the hydrocephalic brain. Analytic solutions for the displacement of brain tissue and the distribution of edema for the annular regions of an idealized cylindrical geometry and small-strain theory are found. The solutions are used for a large-deformation analysis by superposition of the responses obtained for incrementally increasing loading. The effects of structural and hydraulic differences of white and gray brain matter, and the ependymal lining surrounding the venticles, are examined. The results reproduce the characteristic steady-state distribution of edema seen in hydrocephalus, and are compared with experiment. © *1997 Society for Mathematical Biology*

[1]Current address: Institute of Fundamental Technological Research, PAS, Mielzynskiego 27/29, 61-725 Poznan, Poland.

[2]Author to whom correspondence should be addressed. Current address: Chemical Industry Institute of Toxicology, P.O. Box 12137, Research Triangle Park, NC 27709, U.S.A.

1. Introduction. Obstructive hydrocephalus is a disease caused by conditions that obstruct the outflow of cerebrospinal fluid (CSF) from the brain ventricles. It is characterized by significant changes in the water content and transport in the brain. These changes are always accompanied by brain deformation, often large. The purpose of this work is to develop a mathematical model which reproduces both the hydraulic and mechanical changes that occur in a hydrocephalic brain.

The brain ventricles, marked "V" in Fig. 1, are a series of connected cavities in the brain, filled with CSF. CSF, which is mainly composed of water, is largely produced (about 80%) by the choroid plexus that lines the interior of the ventricular walls (Rekate and Olivero, 1990). From there, the CSF flows through the fourth ventricle into the (subarachnoid) space around the spinal cord and the brain, and is absorbed into the venous blood

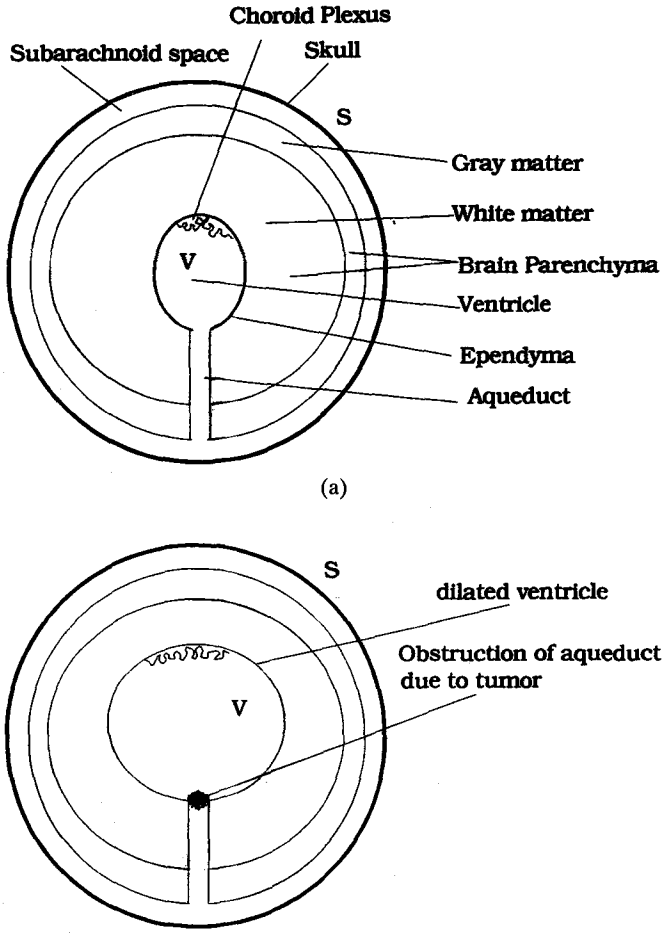

Figure 1. Schematic of the brain. (a) Normal brain; (b) hydrocephalic brain.

through the arachnoid villi. The available data indicate that the CSF is produced at a pressure-independent rate of 0.35 to 0.37 ml/min (Rekate and Olivero; 1990; Nyberg-Hansen *et al.*, 1975). An obstruction of outflow of CSF (as caused by tumors or congenital defects) leads to increased pressure within the ventricles (Fig. 1b). The CSF then flows through alternate pathways, these are widely believed to be through the ventricular walls and into the interstitial spaces of the surrounding brain. Here it flows outward under a pressure gradient and subsequently gets absorbed into the bloodstream through the semipermeable walls of the fine venules distributed largely throughout the gray matter of the brain (Nyberg-Hansen *et al.*, 1975; Lux *et al.*, 1970).

Clinical hydrocephalus has two distinctive features. One is the dilation of the ventricles following the increased ventricular pressure (Figs. 1b and 2b). The second is the movement of fluid out of the ventricles into the brain parenchyma and the development of edema—the accumulation of this fluid in the interstitial spaces of the surrounding brain. The edema is seen as a hypodensity of x-ray computed tomographic (CT) scans or as altered

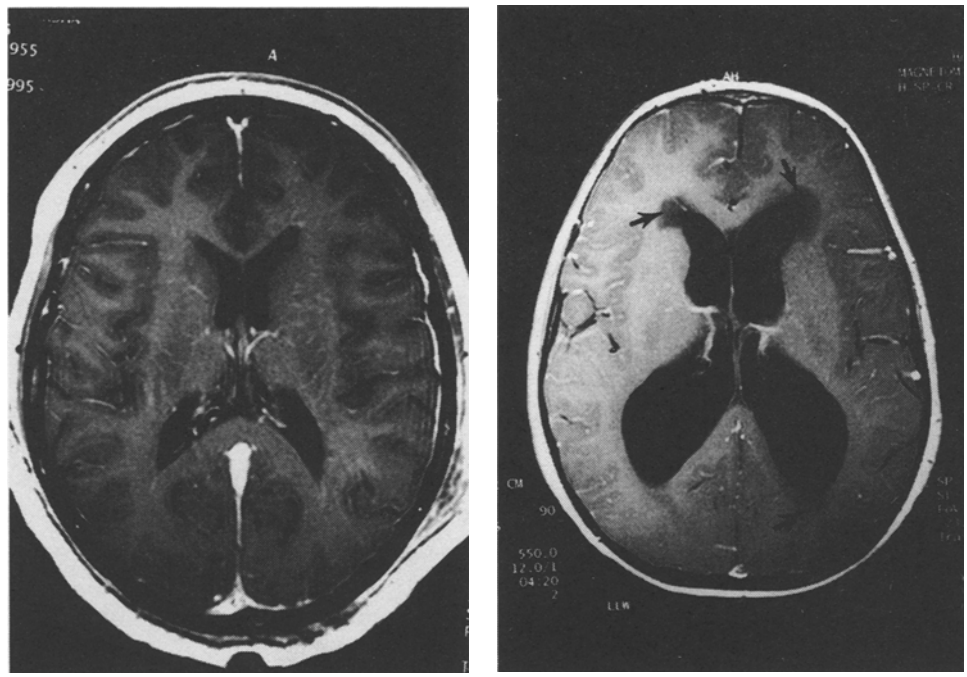

(a) (b)

Figure 2. MRI studies of brain, showing normal and dilated ventricles. (a) Axial image, level of internal cerebral veins. T1-weighted spin-echo axial image showing normal ventricular configuration. (b) Axial image at the level of internal cerebral veins, showing severe dilation of ventricles due to hydrocephalus. The low-density regions marked by arrows indicate increased water content in tissue.

signal-intensity regions in MRI scans of the brain. In severe cases, there is a marked accumulation of fluid all along the ventricular boundary accompanying a large ventricular expansion, as seen in the magnetic resonance image (MRI) scan of Fig. 2b. This characteristically periventricular feature of the edema (Pasquini *et al.*, 1977) is particularly interesting, but unexplained.

Biological tissues are biphasic. Their microstructure can be described as composed of cellular conglomerates embedded in a fibrous extracellular matrix (Oloyede and Broom, 1991); and interstices of this matrix contain water in bound and free states. Biological solids can thus be considered to be porous solids filled with fluid. Under the action of an external load, the deformation of such a solid is accompanied by fluid flow through the porous medium. That the mechanical deformation of the brain is always accompanied by edema suggests that incorporating this biphasic nature is critical to the proper modeling of hydrocephalus and many other problems in brain biomechanics.

In this work, we model hydrocephalus by incorporating the coupled dynamical (viscous) interaction between the fluid flow and the mechanical deformation of the brain tissue. This approach reproduces the specific features of hydrocephalic edema and ventricular dilatation. The geometry of the head is idealized to be that of concentric cylinders, with the brain parenchyma contained in the annular regions. The brain parenchyma is treated as a porous medium whose pore space is saturated with viscous, incompressible fluid. The fluid is considered incompressible since it is largely composed of water. The voids of the solid matrix correspond to the extracellular space of the brain parenchyma (Rall *et al.*, 1962). Such a description is comparable to Hakim's physical analogy of a sponge-like material for brain matter (Hakim and Hakim, 1984). The above conceptualization of the brain takes place in our model at the macroscopic level. While the cells in the solid matrix at the microscopic level are themselves incompressible, the deformation of the porous solid is brought about by porosity changes due to its dynamical interaction with the fluid flow. The general formalism of our approach is known as the theory of mixtures. Specific applications of this approach, called the theory of consolidation or poroelasticity (Biot, 1941), have been extensively used by soil and rock engineers, and have also been used by others to model soft biological tissue when the fluid flow is characterized by a small Reynolds number; for instance, in studies on the deformation of articular cartilage (Oloyede and Broom, 1991), on fluid flow across the arterial wall (Klanchar and Tarbell, 1987; Jayaraman, 1983) and on the behavior of cardiac muscle (Yang and Taber, 1991).

Biot's theory of consolidation has also been used recently to study brain biomechanics. This work furthers the effort of Drake *et al.* (1996), who have obtained closed-form analytic solutions for a cylindrical geometry using a

small-strain approximation and allowing the skull boundary to move. Both these assumptions pose problems in the study of hydrocephalus. The skull boundary in adults is rigid; therefore, the outer boundary of the brain should be considered fixed. The actual displacement of the brain close to the ventricle can be as large as 30 to 40 percent of the total distance between the ventricle and the skull, as evident from comparison of Fig. 2a and Fig. 2b. The extracellular space close to the ventricle is known to expand due to the edema in that region. Since the total vascular volume is only about 3 percent of the total cranial volume (which is a constant), and the fluid and cellular components of the brain are essentially incompressible at physiologic pressures, significant compaction of the brain tissue in regions away from the ventricle must then take place. This is borne out by CT and MRI scans. Thus, there is a large gradient in the tissue deformation, and therefore a large strain. The change in the fluid content in the periventricular region is also large, as seen qualitatively from the edematous regions of Figs. 2b and 3, and quantitatively from Fig. 4, which gives the measured distribution of the increase in water content in the vicinity of the ventricle, based on the experimental results of Lux *et al.*, (1970). The small-strain approximation is thus not reasonable for hydrocephalus.

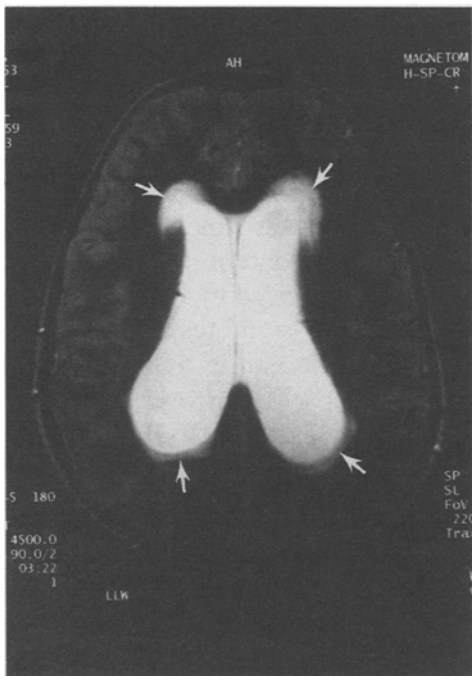

Figure 3. MRI studies of brain, showing edema. T2-weighted spin-echo image showing CSF as bright white, and areas of increased water content in the brain as lesser degrees of whiteness. Periventricular edema is indicated by the arrows.

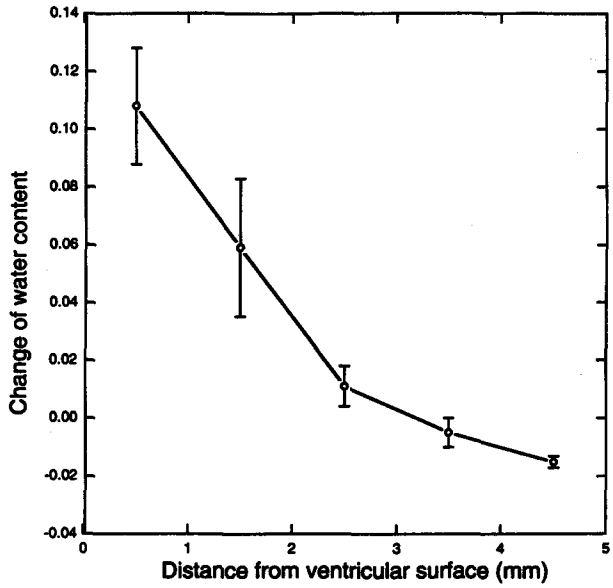

Figure 4. Water content in the hydrocephalic cat. Data from experiment due to Lux *et al.* (1970). Change of water content in the brain of a hydrocephalic cat measured as the ratio of the change in inulin ^{14}C concentration in the extracellular space to the concentration in the ventricular space. See section 3.3 for further details.

The first application of Biot's approach to the brain was by Nagashima *et al.*, (1987, 1990), who developed a finite-element model within the small-strain approximation to study hydrocephalus and vasogenic brain edema. In earlier work, we have obtained finite-element solutions for a similar Biot model to study the progression of the disease in time (Subramaniam *et al.*, 1995). Nagashima's work uses a Poisson ratio of 0.499 for the solid matrix of the porous medium, which makes it nearly incompressible and incapable of sustaining changes in fluid content for realistic values of the elastic modulus. This has also been criticized by Drake *et al.*, who show that such a value leads to physically inconsistent results. The inability to make such approximations pertaining to the strain and compressibility of the porous medium distinguishes the study of hydrocephalus from problems such as atherosclerosis (Klanchar and Tarbell, 1987). The large-displacement issue applies to brain biomechanics in general, as similar changes occur in cerebral hemorrhage and in the edema that follows the breakdown of the blood-brain barrier in trauma and tumor growth. The study of hydrocephalus therefore provides an excellent testing ground for the validity of accurate solid-fluid "mixture" theories to be used for the study of brain biomechanics as well as for other biological tissues.

In this work, we demonstrate that the important features of the hydrocephalic brain are distinctly that of a porous material undergoing deformation due to fluid flow. We have formulated a numerical scheme for a

large-deformation analysis; our results show the error arising from a small-strain approximation. We have incorporated the structural and hydraulic differences of gray and white matter, and the ependymal lining surrounding the ventricles, and have examined their effect on the edema and ventricular dilation. A velocity boundary condition is used based upon known values of the CSF production rate, in contrast to the pressure boundary condition used by Drake *et al.*, (1996) and Nagashima *et al.*, (1987, 1990).

In the next section, we detail the model and its underlying assumptions. The model is then solved within a small-strain theory. Next, the solutions are extended to incorporate a strain dependence in the permeability. In section 3, we describe a formulation to treat large deformations using these solutions. This is followed by a discussion of the parameters used and quantitative results. The distribution of water content obtained by our model is compared with experiment. The Appendix elaborates further upon the significance of the parameters used in poroelastic theories.

2. The Model.

2.1. *General assumptions.* In this model, schematized in Fig. 1a and 1b, we presume that the CSF is formed entirely within the ventricles and that the disease state is produced by complete occlusion of the aqueduct (outflow tract) by, for example, a small tumor. Following occlusion, the CSF (in the model) seeps into the surrounding parenchyma and flows through it. Here, we idealize that all absorption of the CSF takes place at the edge of the subarachnoid space. This edge, in our model, is equivalent to the skull boundary.

The brain consists largely of two types of tissue—gray matter, containing nerve cell bodies and their dendritic processes, and white matter, characterized by a large proportion of myelinated axons (Hirano, 1993). Gray matter, comprising about 30% of the total brain volume, is mostly found at the periphery of the brain and has a much higher concentration of blood vessels. In the white matter, each axon is encased in many layers of myelin sheath provided by an oligodendroglial cell membrane. Thus the white matter consists, to a large extent, of water-permeable lipid bilayer structures. In contrast, the cell bodies, dendrites and blood vessels in the gray matter contain numerous tight junctions, gap junctions and synaptic clefts, all structures with tightly regulated permeability. Furthermore, the cellular elements of gray matter are highly intermingled, in contrast to white matter, which has an orderly arrangement of nerve fibers running in roughly parallel fashion (Hirano, 1993). Consequently, as argued by Reulen *et al.* (1977), the extracellular space of gray matter offers more structural resistance to enlargement than white matter; we have modeled this by considering a low permeability for gray matter.

The edge of the ventricular boundary is lined by a thin layer of cells known as the ependyma, which is permeable to CSF (Nag, 1991). The cells in this layer are, however, packed closely together and the extracellular space is diminished relative to that of the brain parenchyma. We therefore assume that the permeability of this structure is less than that of the white matter of the brain. The ependyma is also observed to be structurally stiffer than the rest of the brain tissue. Although the thickness of the ependyma is about 0.5 mm, this is much smaller than its radius. Thus, neglecting inhomogeneities of the stress in the solid matrix of the ependyma and in the fluid velocity through it, we adopt a membrane model for the ependyma.

The brain parenchyma and the ependyma are modeled as a two-phase medium composed of a porous elastic matrix saturated with fluid. The constitutive equations for the model refer to the macroscopic behavior, i.e., each local quantity (fluid velocity, matrix displacement, stresses, etc.) is understood as an average of the corresponding microscopic quantity. The averaging is assumed to be over a length-scale much larger than the characteristic size of the pores; it therefore disregards inhomogeneities at the microstructure level. On the other hand, the averages are over domains much smaller than the size of the brain, thus allowing a continuum approach.

To permit solving the coupled differential analytically, we have represented the brain geometry as a thick-walled cylinder with a central cavity which represents the ventricular space at whose edges the boundary conditions are specified. The brain parenchyma is contained in the annular region of the cylinder. Other model-specific neuroanatomical distinctions are also made as explained below.

We consider three cases. First, we presume a homogeneous material for the entire brain parenchyma (that is, a single annular region). In the second case, we admit different mechanical and hydraulic properties for white and gray matter of the brain. We split the annular region into two adjoining rings. The outer annular region corresponds to gray matter, the inner annular region to white matter. The two regions mechanically interact at their interface. We will refer to the above cases as the "single ring" and "double ring" models, respectively. In the third case, we add, to the double ring model, a membrane representing the ependymal lining at the ventricular boundary. This membrane is stiffer and has a lower permeability than white matter.

With reference to Fig. 1a, the boundary conditions are as follows:

1. At the outermost boundary, S, the displacement of the solid and the fluid pressure are zero. The former condition corresponds to a rigid adult skull, while the latter implies the reference pressure to be zero. The velocity of fluid at the skull boundary is constant and such that it corresponds to the fluid production rate within the ventricle (0.37

ml/min for adults). We believe this is superior to using ventricular pressure as the boundary condition since the production rate is known with a greater level of accuracy and, furthermore, is considered to not vary with pressure.

2. At the ventricular boundary, V, continuity of stress in the fluid is assumed. The displacement at this boundary is not constrained.

2.2. *Two-phase model of brain tissue.* The basic principles of the two-phase mechanical model of saturated porous media are the balances of mass and linear momentum. These are established independently for each phase α ($\alpha = s$ for solid and $= f$ for fluid) (see, Bowen, 1976; Kenyon, 1976), i.e.,

$$\frac{\partial(n^\alpha \rho^\alpha)}{\partial t} + \nabla \cdot (n^\alpha \rho^\alpha \mathbf{v}^\alpha) = m^\alpha, \tag{1}$$

$$\frac{\partial(n^\alpha \rho^\alpha \mathbf{v}^\alpha)}{\partial t} + \nabla \cdot (n^\alpha \rho^\alpha \mathbf{v}^\alpha \mathbf{v}^\alpha) - \nabla \cdot \sigma^\alpha - n^\alpha \rho^\alpha \mathbf{b}^\alpha = \mathbf{R}^\alpha. \tag{2}$$

n^α, ρ^α, and $\mathbf{v}^\alpha$ denote volume fraction, intrinsic mass density, and velocity of phase α. σ^α and $\mathbf{b}^\alpha$ are stress tensor and density of external body forces. m^α and $\mathbf{R}^\alpha$ are rate of mass and linear momentum exchange between the two phases. Since we have a closed mass system, the equations must satisfy the relations

$$m^s + m^f = 0, \tag{3}$$

$$\mathbf{R}^s + \mathbf{R}^f = \mathbf{0}. \tag{4}$$

We are interested in the steady-state behavior of the brain body; therefore, the inertial forces are neglected, no mass exchange between phases is allowed, and solid velocity should be equal to zero. Then, for a constant intrinsic density of the fluid, the system of four balance equations (1), (2) may be reduced to three steady-state equations, which for convenience are rearranged using conditions (3) and (4), to the form

$$\nabla \cdot \mathbf{q} = 0, \tag{5}$$

$$\nabla \cdot (\sigma^s + \sigma^f) = \mathbf{0}, \tag{6}$$

$$\nabla \cdot \sigma^f + \mathbf{R}^f = \mathbf{0}, \tag{7}$$

where $\mathbf{q}(= n^f \mathbf{v}^f)$ is the rate of volumetric flow or discharge velocity of fluid.

The brain material is subjected to drained conditions, where the flow of fluid out of the loaded porous material is possible. Since the bulk modulus of the brain matter is much smaller than the compressibility of the solid

tissue itself, we may adopt Terzaghi's principle of effective stress (Kumpel, 1991). The effective stress, σ', is defined as the difference between the total stress, $\sigma^s + \sigma^f$, and the hydrostatic component of intrinsic pore fluid stress, $-p$. Terzaghi's principle uniquely relates the effective stress to the strain of the solid matrix (Detournay, 1993). That is, if we disregard the contribution of the viscous interaction in the fluid to the macroscopic stress tensor, as assumed for flow through most porous materials (Atkin and Craine, 1976), then for small deformations of an isotropic material, the stress state can be expressed by the equations

$$\sigma^f = -np\mathbf{I}, \tag{8}$$

$$\sigma' = \sigma^s + \sigma^f + p\mathbf{I} = 2\mu\mathbf{e} + \lambda \operatorname{tr}\mathbf{e}\,\mathbf{I}, \tag{9}$$

where $n(=n^f)$ is porosity of the material. The pore pressure, p, is taken to be positive when compressive, in contrast to the opposite sign convention for stresses. The small-strain tensor $\mathbf{e}$ is related to the displacement of the solid matrix $\mathbf{u}$, $\mathbf{e} = \frac{1}{2}[\nabla\mathbf{u} + (\nabla\mathbf{u})^T]$, and μ and λ are the Lamé constants of the brain matter under drained conditions. The interaction force, $\mathbf{R}^f$, for the steady flow of fluid through porous materials has two components: the term representing viscous interaction of fluid with solid matrix, and the buoyancy force due to the variable volume fraction of phases (Bowen, 1976), i.e.,

$$\mathbf{R}^f = -\frac{\mu^f n}{k}\mathbf{q} + p\nabla n. \tag{10}$$

μ^f is the dynamic viscosity of the fluid, and k is the intrinsic permeability of the solid. It may be noted that one can obtain Darcy's Law in this theory from equations (7) and (10).

The change in the water content per unit volume of the porous sample is equal to the dilatation ($\operatorname{tr}\mathbf{e}$), if the density of the solid is assumed to be constant. Since the deformation of the solid matrix of the soft brain matter induces a change in its microstructure, the permeability of the material is, in general, a function of deformation. Mow *et al.*, (1980) have demonstrated the validity of the following two-parameter model in their study of small strains of articular cartilage:

$$\frac{1}{k} = \frac{1}{k_0}(1 - M \operatorname{tr}\mathbf{e}), \tag{11}$$

where k_0 and M are constants. This was later used by Klanchar and Tarbell (1987) while studying water transport through arterial walls. The above expression is a small-strain approximation of a more general exponential

relationship for permeability. For the case when the parameter M is assumed to be small, this is equivalent to the assumption of a constant permeability. Although the principal structural protein in cartilage is collagen, a triple α-helix, while in the brain the principal long structures are neurofilaments and neurotubules, non-destructive deformation of either tissue must be limited to bending and stretching of long proteins without breaking covalent or hydrogen bonds. We therefore postulate that the relationship given above should apply as well to brain tissue in the reversible deformation domain.

2.3. *Membrane model for the ependyma.* We model the ependyma as a two-phase cylindrical membrane (two-dimensional body). The principle of mass conservation requires the continuity of discharge velocity, $\mathbf{q}$, through the membrane, i.e. $\mathbf{q}^+ = \mathbf{q}^-$, where $+$ and $-$ refer to the internal and external boundaries of the membrane. The balance of radial components of linear momentum of the solid and fluid components for any small element of the membrane gives us (see Appendix for details),

$$\sigma^e - (\sigma^+ - \sigma^- + R^{fe}) r^v = 0, \tag{12}$$

$$-(p^+ - p^-) n_e + R^{ef} = 0. \tag{13}$$

Here, σ^e is the circumferential component of the membrane stress, σ^+ and σ^- are normal components of the stress vectors on solid matrix, defined on the external and internal surfaces of the cylindrical membrane, and r^v is the radius of the cylinder. R^{fe} $(= R^{ef})$ denotes the interaction force between the fluid and the membrane matrix, n_e is the membrane porosity, and p^+, p^- refer to the fluid pressure on the membrane surfaces.

Assuming that the membrane stress is linearly dependent on the stretching of the membrane, one obtains a linear relationship between surface stress, σ^e, and radial displacement of the membrane, u_e,

$$\sigma^e = \alpha_e \frac{u_e}{r^v}, \tag{14}$$

where α_e is the elastic modulus of the membrane. The interaction force between fluid flowing through the membrane and the membrane matrix, R^{fe}, is assumed to be proportional to the velocity of fluid flowing through the membrane,

$$-R^{fe} = R^{ef} = -\frac{u^f n_e}{k_e} q_e, \tag{15}$$

where the permeability of the membrane, k_e, is represented in the form assumed for the brain parenchyma, i.e.,

$$\frac{1}{k_e} = \frac{1}{k_{e0}}\left(1 - M^e \frac{u_e}{r^v}\right), \tag{16}$$

and k_{e0}, M^e are constants.

The components of stress on the internal and external surfaces of the cylindrical membrane are determined by the fluid pressure in the ventricles, p^-, and the stress tensor in the brain matrix, σ^s, respectively. Hence, assuming that the porosity of the membrane is equal to the porosity of the adjoining brain ($n_e = n$), we have that

$$\sigma^- = -(1-n)p^-, \tag{17}$$

$$\sigma^+ = \sigma_v' - (1-n)p^+, \tag{18}$$

where σ_v' is the radial component of the effectiveness stress in the adjoining brain tissue. Eliminating the stresses, pressures and interaction forces, the above equations lead to the condition

$$\frac{\alpha_e}{(r^v)^2}u_e - \sigma_v' + q_e \frac{\mu^f}{k_e}\left(1 - M^e \frac{u_e}{r^v}\right) = 0. \tag{19}$$

The above equation determines the equilibrium condition of the membrane and will be used in case 3 as a boundary condition at the inner boundary and the annular region.

2.4. *Analytical solutions.* Assuming that all dependent variables of the two-phase model of brain matter, i.e. fluid velocity, fluid pressure and solid displacement, depend only on the radial coordinate r (axial symmetry), and using constitutive functions defined by relations (8)–(11), the governing equations, (5)–(7), reduce to the following system of ordinary differential equations in cylindrical coordinates:

$$\frac{dq}{dr} + \frac{q}{r} = 0, \tag{20}$$

$$(2\mu + \lambda)\left(\frac{d^2u}{dr^2} + \frac{1}{r}\frac{du}{dr} - \frac{u}{r^2}\right) - \frac{dp}{dr} = 0, \tag{21}$$

$$\frac{dp}{dr} + \frac{\mu^f}{k_0}\left[1 - M\left(\frac{du}{dr} + \frac{u}{r}\right)\right]q = 0. \tag{22}$$

Integration of equation (20) gives

$$q = \frac{C_1}{r}, \tag{23}$$

where C_1 is an integration constant. Substitution of equations (23) and (22) into equation (21) leads to the following non-homogeneous differential equation with variable coefficients:

$$r^2\frac{d^2u}{dr^2} + Br\frac{du}{dr} - Cu = -\kappa r, \tag{24}$$

where the new parameters B, C and κ are defined as follows.

$$B = 1 - \frac{\mu^f M C_1}{(2\mu + \lambda)k_0}, \qquad C = 1 + \frac{\mu^f M C_1}{(2\mu + \lambda)k_0}, \qquad \kappa = \frac{\mu^f C_1}{(2\mu + \lambda)k_0}. \tag{25}$$

The solution of equation (24) can be found as the sum of the general solution of the homogeneous equation (of the Cauchy-Euler type), u_h, and of a particular solution of the non-homogeneous equation, u_n (see, e.g., Rabenstain, 1972). This solution is

$$u = u_h + u_n + C_2(r)^{v_1} + C_3(r)^{v_2} - \frac{\kappa}{B - C}r, \tag{26}$$

where C_2 and C_3 are integration constants, and v_1 and v_2 are roots of the algebraic equation $v^2 + (B-1)v - C = 0$.

Using solutions (23) and (26) in equation (22) and then integrating the resulting equation, we finally obtain a formula for the radial distribution of fluid pressure:

$$p = \frac{\mu^f C_1}{k_0}\left[-\left(1 + \frac{2\kappa M}{B - C}\right)\ln r + MC_2\frac{v_1 + 1}{v_1 - 1}(r)^{v_1 - 1} + MC_3\frac{v_2 + 1}{v_2 - 1}(r)^{v_2 - 1} + C_4\right], \tag{27}$$

where C_4 is the fourth integration constant of the boundary value problem.

2.5. *Boundary and matching conditions.* Solutions (23), (26) and (27) contain four unknown integration constants C_1–C_4. Thus, to find the final form of the solutions for the single homogeneous ring of the brain matter, four boundary conditions are required. Subsequently, boundary conditions

valid for all of the considered geometries will be specified. The detailed forms of the integration constants for the three geometries are determined on the basis of these conditions and are given in the Appendix.

We have the following conditions at the outer (skull) boundary of the brain for all the three models: (1) displacement of the solid is zero, (2) the fluid pressure is equal to zero, and (3) the discharge velocity of the fluid is a given constant Q, i.e.,

$$u = 0, \qquad p = 0, \qquad q = Q \qquad \text{for} \quad r = r^s. \tag{28}$$

The axial symmetry of the problems permits us to consider a uniform pressure and velocity at this boundary. Further note that the symmetry also allows us to prescribe the discharge velocity at the outer boundary, instead of specifying it at the inner ventricular boundary.

At the inner (and interfacial, for cases II and III) boundary, we have for the three models:

(I) *Single ring model.* The total stress at the inner (ventricle) surface of the ring, $r = r^v$, is determined by the pressure in the ventricles. In our analysis, this is an unknown. However, by virtue of the effective stress principle, the effective stress at this boundary is prescribed equal to zero,

$$\sigma_v' = 0 \qquad \text{for} \quad r = r^v. \tag{29}$$

(II) *Double ring model.* The two adjoining concentric regions are in general characterized by different values for the elastic constants and permeabilities. Then, the solutions (23)–(27) are valid within the inner and outer rings, and two sets of integration constants (eight parameters) need to be determined.

The boundary conditions (28) and (29) are still valid. Matching conditions are then specified at the interface between the two rings at $r = r^i$, and result from continuity requirements for the displacement of the solid matrix, the mass flux of fluid, pore pressure and the effective stress, i.e.,

$$u^w = u^g, \qquad q^w = q^g, \qquad p^w = p^g, \qquad \sigma^w = \sigma^g \qquad \text{for} \quad r = r^i. \tag{30}$$

(III) *Double ring lined with permeable membrane.* The system of two rings, as considered above, is assumed to be lined with an elastic permeable membrane, as described in section 2.3. Since the membrane is assumed to be a two-dimensional continuum, equation (19), which is derived from the equilibrium condition of the membrane, may be used as the boundary condition for the inner surface of the inner annular region. This condition replaces condition (29) in the set of boundary conditions of case II.

3. Results and Discussion.

3.1. *Material parameters.* The numerical implementation of our model requires the specification of two parameters describing elastic properties and permeability for the brain material in each of the annular regions as well as in the ependymal membrane (the numerical data are given in Table 1). The elastic properties of the skeleton under drained conditions are specified by the Young's modulus, E, and Poisson's ratio, ν. The Lamé constants μ and λ, used in section 2 to define the elastic properties of the porous brain, are related to parameters E and ν: $\mu = E/[2(1+\nu)]$ and $\lambda = E\nu/[(1+\nu)(1-2\nu)]$. We use the value determined by Metz *et al.* (1970) for E. Since the phenomenon being studied is very slow, we use the value determined for the lowest strain in this reference. Drake *et al.* (1996) have reassessed Metz's experimental data for use in poroelastic calculations. We use their rough estimate of 0.35 for ν. Their suggested value of E is in agreement with that used in our calculation. The conditions under which the above parameters are valid are examined further in the Appendix.

As the solid matrix deforms, the change in porosity induces a corresponding change in the permeability of the medium. This is likely to be particularly significant for the ependyma, for it is known that the development of extensive edema in hydrocephalus does not take place until a moderate amount of "flattening and tearing" of this membrane has occurred (Nyberg-Hansen *et al.*, 1975). We have incorporated a dilatation-dependence in the functional form for the permeability (section 2.2) and presented results for the small-strain case. However, we have been unable to include this feature in the numerical solutions obtained for large deformations; this is discussed further in the Results section. Thus the numerical results we present for large deformations use a constant value for the permeability

Table 1. Material parameters

Model	Elastic modulus [N/m^2]	Poisson's ratio [—]	Permeability [m^4/N s]
Case I.			
White matter	$1.0\cdot10^4$	0.35	$1.6\cdot10^{-11}$
Case II.			
White matter	$1.0\cdot10^4$	0.35	$1.6\cdot10^{-11}$
+gray matter	$1.0\cdot10^4$	0.35	$1.6\cdot10^{-13}$
Case III.			
White matter	$1.0\cdot10^4$	0.35	$1.6\cdot10^{-11}$
+gray matter	$1.0\cdot10^4$	0.35	$1.6\cdot10^{-13}$
+ependyma[a]	$5.0\cdot10^5$		$1.0\cdot10^{-12}$

[a]To get the elastic modulus, α_e, and permeability of the membrane, k_e, defined in the model (section 2.3), the values given in the table must be multiplied and divided, respectively, by the thickness of the membrane, equal to 0.05 cm.

within each homogeneous annular region and the ependymal membrane. The value used for the permeability of white matter is calculated from the work by Reulen *et al.* (1977) on the spread of Na-fluorescein dye through the brain in cold-induced edema. As discussed earlier, the permeability of gray brain matter is expected to be significantly lower than that for white matter. We have therefore chosen a value smaller by two orders of magnitude than that for the inner ring.

The radii for the different annular regions are chosen to roughly correspond to their locations in adult human brains. In the absence (to the best of our knowledge) of experimental data for the hydraulic and mechanical parameters for the ependymal membrane, we have chosen values for the elastic modulus and permeability that, in comparison with white matter, make the ependyma stiffer by a factor of 50 and less permeable by a factor of 10.

3.2. *Small-deformation analysis.* If the discharge velocity specified at the outermost boundary, Q, is small enough that the relative deformation of the brain body does not exceed a few percent, the small-strain solutions given by equations (23), (26) and (27) may be used to quantify the hydromechanical behavior of the brain. Figure 5 shows the dilatation of the brain matrix, defined as $du/dr + u/r$, vs radius for the three considered geometries. The value of Q for the small-deformation analysis is chosen to be 100 times smaller than the velocity $39.3 \cdot 10^{-6}$ cm/s, determined from the experimentally assessed production rate of the CSF (Rekate and Olivero, 1990). Following the data for articular cartilage (Klanchar and Tarbell, 1987), the parameters M^w, M^g and M^e, which describe the dependence of permeability of the materials in the three regions on their deformation, are assumed to be equal to 4.3.

The radial flow of CSF through permeable brain matter induces an interaction force between the fluid and the solid brain matrix (see section 2.2), experienced by the solid as a mechanical loading. This results in an outward displacement of elements of the brain material. Because of the zero displacement boundary condition at the outermost (skull) surface, the material in the annular region experiences a bulk compression. On the other hand, however, for the cylindrical geometry considered here, the radial displacement of solid elements is necessarily accompanied by their circumferential stretching. The local state of strain and the distribution of dilatation of the matrix, which in turn represents the change in water content of the brain, are thus determined by the increment of the radial displacement and the displacement itself. The calculated distribution of dilatation of the porous brain matrix, given in Fig. 5, shows that for all the models, the volume of the material in the inner part of the brain ring increases, with the greatest increase occurring at the periphery of the

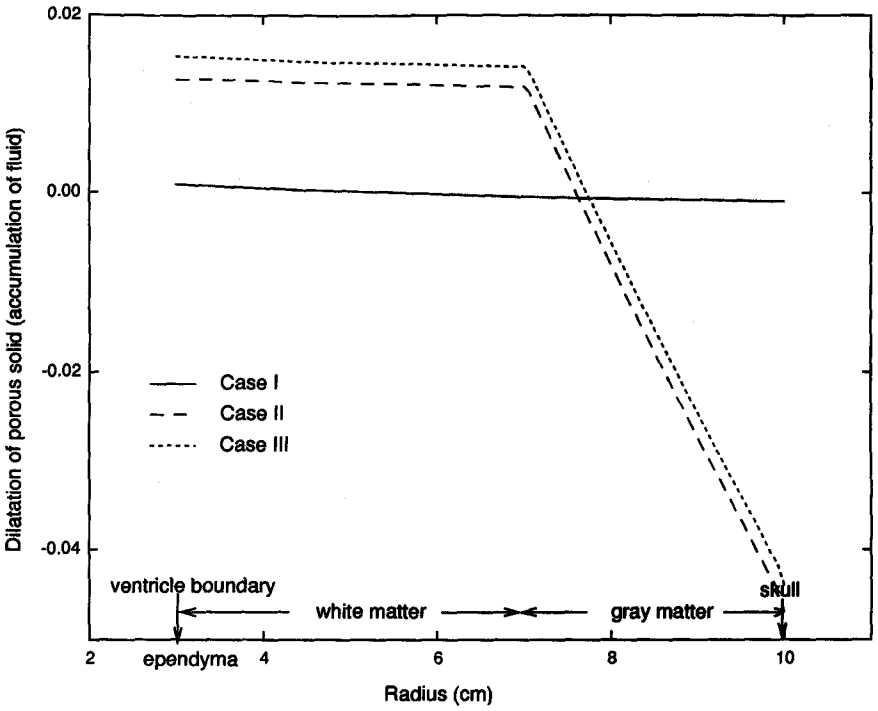

Figure 5. Calculated dilatation for the small-strain case. This represents the change in fluid content. Case I: white matter only, case II: white and gray matter; case III: case II + ependymal membrane.

ventricle. This explains the increased edema measured experimentally, and seen in MRI scans, near the ventricles. The material in the outer part of the brain ring decreases in volume, and the magnitude of the volume change depends mainly on the permeability of the material.

3.3. *Large-deformation analysis.* The small-strain model is valid only for small fluid velocities since the driving force of deformation of the brain matrix is the fluid flow. Thus, the small-strain model is applicable only to a partial occlusion of CSF outflow and, therefore, to ventricular dilatations far smaller than those in Fig. 2b.

Following methods used in computational mechanics, we develop solutions pertaining to large-deformation cases by superposition of the small-strain solutions. Such an approach is an alternative to large-strain theory, which uses the full non-linear form of the strain tensor (geometrically non-linear model). Under the scheme used in this work, the loading, that is, the total fluid velocity at the outer boundary of the brain ring, Q ($= 39.3 \cdot 10^{-6}$ cm/s), is divided into a number of equal increments (steps) constituting elementary loadings for each step. For large N, successive iterations of

the small-strain model will converge to the large-deformation result. The value of N deemed sufficient is determined from the convergence criteria of the numerical results for increasing N.

To determine the spatial distribution of the dependent variables, the annular ring is divided into a number of cylindrical elements having the same thickness in the initial configuration. The positions of the inner boundary and the grid formed by the cylindrical elements constitute the finite set of spatial coordinates for which solutions for displacement of the solid matrix, pore pressure and fluid velocity (equations (26), (27), and (23), respectively), corresponding to an incremental increase in the velocity are found. After each incremental loading, the new positions of the chosen set of radial coordinates are determined by the displacement of the matrix, and the boundary and matching conditions are updated. Finally, the changes in the surface area of the small cylindrical elements with respect to their initial surface area are used to determine the ultimate distribution of dilatation of the solid matrix.

The small-strain solution, described in section 3.2, incorporates a functional dependence of the permeability on the dilatation. However, direct application of that function in the above numerical approach for large brain deformations would link the permeability to the dilatation of the solid reached in a single incremental step, and not to the actual dilatation of the matrix. Therefore, our numerical simulations of the large-deformation model will only use constant permeabilities for brain matter in the two annular regions and in the ependyma.

The numerical procedure described above allows calculation of the distributions of displacement, dilatation and pore pressure for the three cylindrical models in the large-deformation range. Figure 6 illustrates the rate of convergence of our solutions and shows that 100 iterations (velocity increments) are enough to obtain convergence in the large-deformation regime. The rate of convergence is similar for all the models. Since the small-strain solution is approximately that obtained for a single iteration of the large-displacement analysis, the results in this figure show that a small-strain analysis can significantly overestimate the displacement (in this case, by a factor of 5).

The final displacement of the brain matrix as a function of radius in the undeformed state is shown in Fig. 7. The ventricular displacement is to be compared with Fig. 2b. The single ring model underestimates the ventricular displacement, whereas the case of complete outflow obstruction should result in a severe form of the disease. The double ring model results in large deformations; since the fluid velocity at the outer boundary is fixed, the low permeability of the gray matter material results in a greater force at the inner boundary. The displacement of the ventricular boundary decreases to less than half of this value when the ependymal membrane is added, as a result of the lower permeability and stiffer structure at the

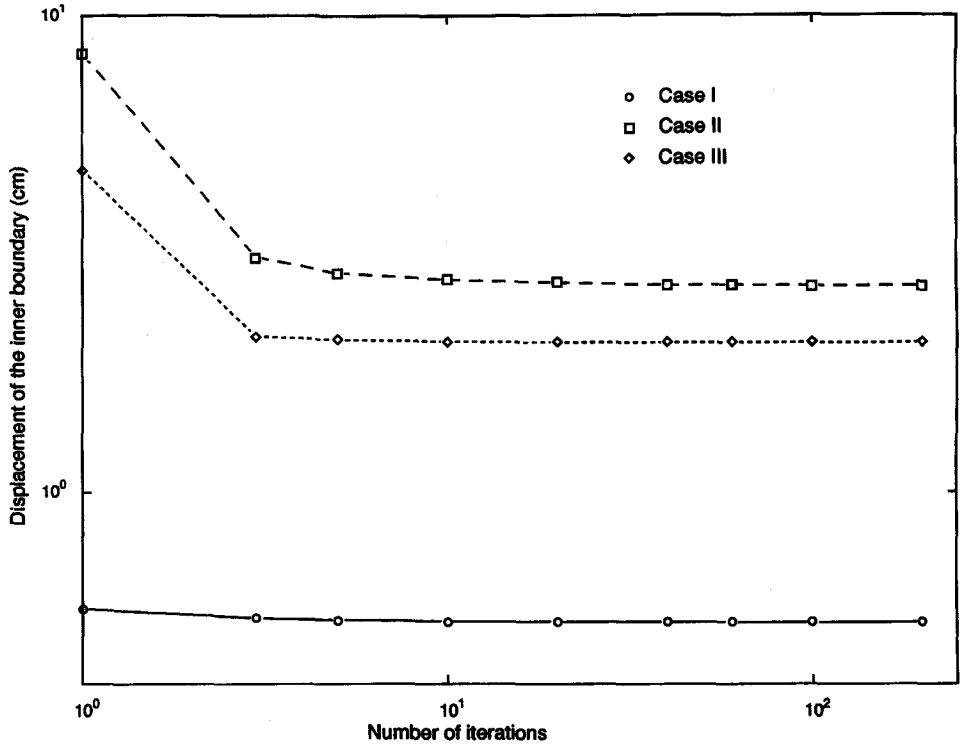

Figure 6. Convergence of solution. Radial displacement vs number of iterations.

ventricular edge. Although the role of the ependyma in brain biomechanics is poorly understood, it is clear that if the parameters we have chosen for the ependyma are qualitatively correct, its inclusion in the model results in a large difference. Our results demonstrate that its effect upon ventricular dilation may be substantial. The ependyma may therefore play an important role in the biomechanics of the brain when significant exchange of CSF takes place with the ventricular space.

Figure 8 shows the distribution of dilatation of the solid matrix as a function of the radius of the undeformed geometry. In all cases, the porous material in the elements near the ventricle increases in volume. Assuming insignificant changes in the density of the solid material, this volumetric expansion of the matrix is equivalent to the increase of the fluid content in the brain material. This demonstrates the formation of extracellular edema, the accumulation of fluid in the extracellular spaces of the tissue. The simulation reproduces the characteristic periventricular nature of hydrocephalic edema seen in Fig. 3, and discussed in the Introduction. The comparison of increments of the displacement of white and gray matter in the double ring models indicates that gray matter undergoes much larger deformations than white matter, resulting in a compaction of the outer ring

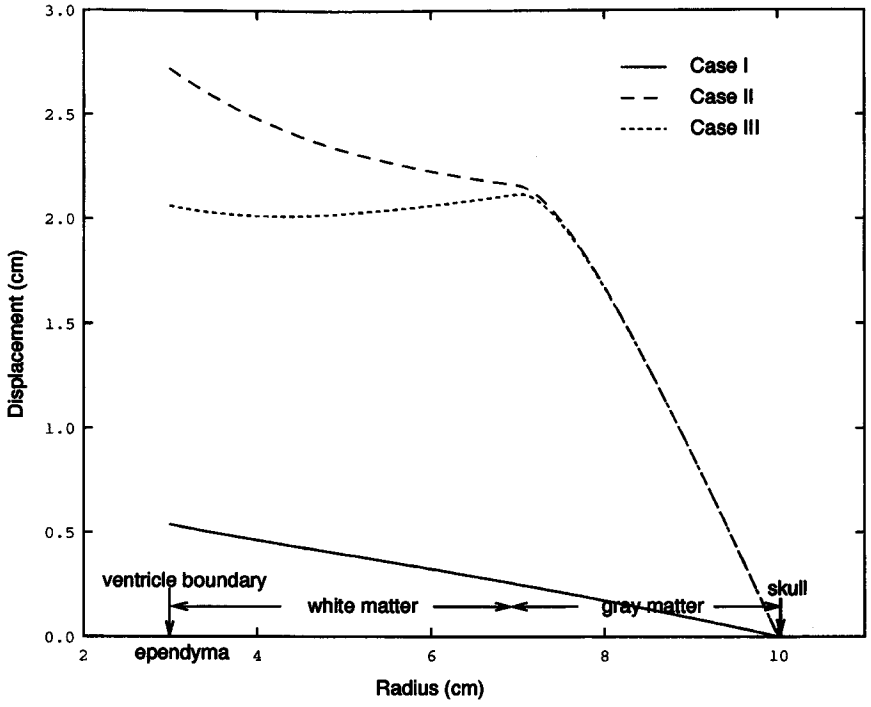

Figure 7. Radial displacement vs distance from ventricular surface.

material. The results show that the formation of edema is almost entirely confined to white matter, in agreement with experimental and clinical observation (Reulen *et al.*, 1977; Weller and Mitchell, 1980). The above observation are, of course, a consequence of the significant difference in the hydraulic properties of the two materials. The negative values for the dilatation indicate the loss of extracellular space. Such a compaction of gray matter is often observed in CT scans of hydrocephalic patients in areas of the brain close to the subarachnoid boundary.

Figure 8 is in good qualitative agreement with the experimental data of Fig. 4, values obtained by Lux et al. (1970) for the distribution of the change in the water content of the brain tissue near the brain ventricles of hydrocephalic cats. The experimental curve has been corrected here to show only the excess extracellular water content relative to the normal cat for the purpose of comparison with our result.[1] A strict quantitative comparison with Fig. 4 is not appropriate since our geometrical dimensions correspond to that of humans.

[1]We have plotted Fig. 4 using the data from Table 2 of their work, which provides the inulin ^{14}C concentration in brain tissue at short distances away (0 to 5 mm) from the ventricle. This is considered a measure of the extracellular space, and therefore that of the water content in the tissue. To obtain the change in water content from their data, we corrected the inulin ^{14}C concentration in the extracellular space of the hydrocephalic cat by that measured in the normal animal. The result is weighted by the concentration in the ventricular space.

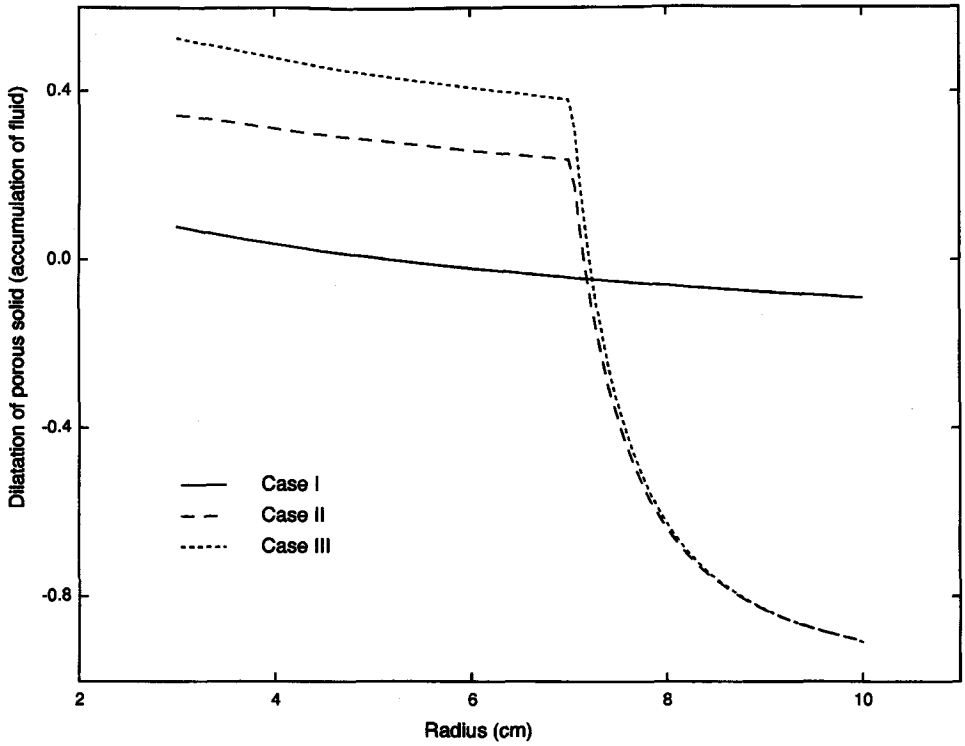

Figure 8. Dilatation vs distance from venticular surface. The dilatation represents the change in fluid content.

The calculated pore pressure distribution shown in Fig. 9 indicates in case I a fluid pressure of 2746 N/m^2 (20.6 Torr) at the ventricular boundary relative to the skull boundary. This is in the range of observed intraventricular pressures in human hydrocephalus. The model demonstrates that this fluid pressure in the ventricles results from the boundary conditions of section 2.5. There is a large difference between this value and that predicted by cases II and III (which obtain almost the same ventricular pressure), a consequence of the low permeability of gray matter. This is, however, not physiologic; the discrepancy arises because of the idealization in our model that all CSF absorption takes place at the skull (subarachnoid) boundary. The absorption is instead believed to be through the capillary bed distributed mainly throughout the gray matter region (Lux *et al.*, 1970).

We next examine the sensitivity of the calculation of the two structural parameters, the Poisson's ratio ν and the elastic modulus E. Figures 10 and 11 compare the displacement distribution for case III for different values of ν and gray matter E. The displacement shows high sensitivity to values of ν greater than 0.45. The displacement at the ventricle increases significantly (by a factor of 2.3) as the elastic modulus of gray matter is increased to four

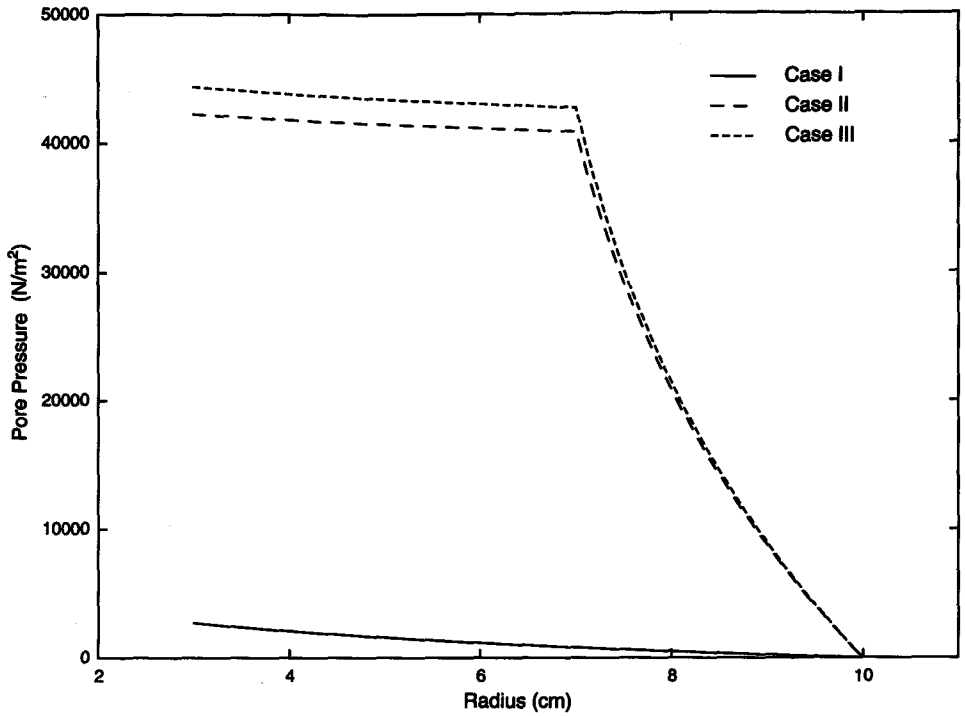

Figure 9. Pressure vs distance from ventricular surface.

times that of white matter. As discussed earlier, we expect gray matter to be structurally stiffer than white matter. Thus the sensitivity analysis underscores the importance of better experimental data on the differences in the elastic moduli, and on the proper range of the Poisson's ratio.

4. Conclusions. A mathematical model was developed for the steady state of the disease, hydrocephalus, based upon a theory of a deformable fluid-filled porous medium for the brain material. The simulations, using a simple geometry and rough estimates of material properties, show that the salient biomechanical features of hydrocephalus result from the response of the brain to well-understood mechanical forces. The model incorporates the interaction between the cerebrospinal fluid flow and the solid matrix of the porous medium. The agreement of our results with experimental and clinical observations demonstrates that this interaction accurately represents the mechanical loading on the matrix which gives rise to the large observed deformations. Further, the model predicts the formation of hydrocephalic edema (accumulation of interstitial fluid) and its characteristic distribution around the brain ventricles, in agreement with experimental data on the edema of hydrocephalic cats. The numerical formulation addresses large deformations, and we demonstrate that a small-strain analysis markedly overestimates the displacement.

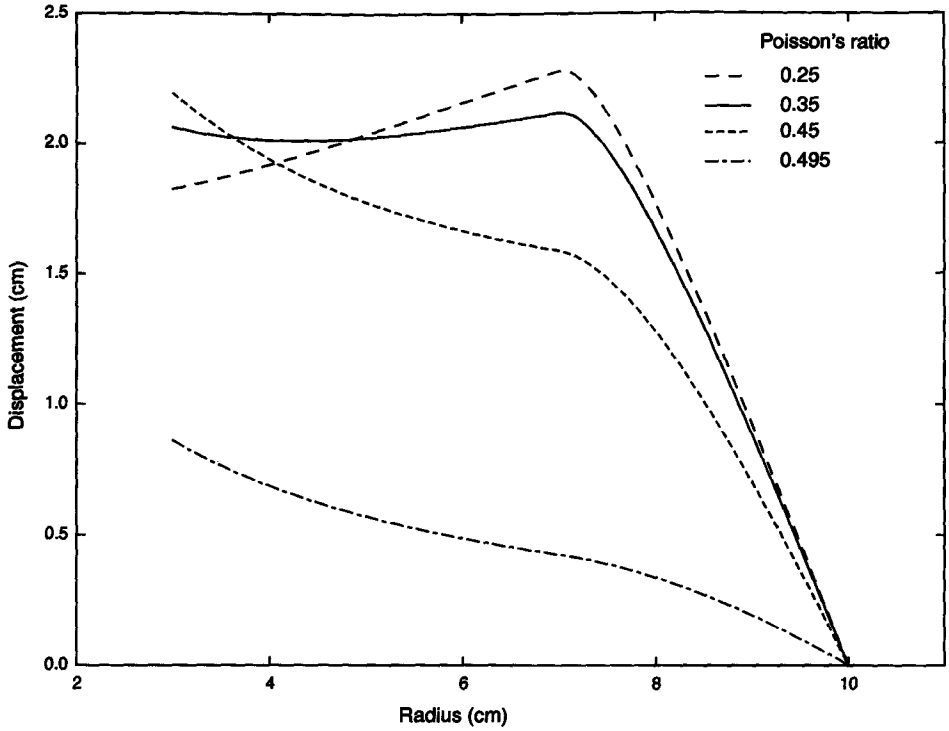

Figure 10. Radial displacement vs distance from ventricular surface for different Poisson's ratios.

We have presented solutions for three cases of the above model. The first case considered a homogeneous annular ring of brain matter; this was enhanced first to include annular regions of gray and white matter and then the ependymal layer around the ventricle. The comparative studies reveal that the structural and hydraulic differences of these regions strongly influence the quantitative results. Experimental data on these differences and for the Poisson's ratio of brain matter are lacking. Our results indicate that experiments focused on determining these values are necessary for realistic simulations of brain biomechanics. Another experimental issue which needs to be addressed is that currently available data have not been determined under the near-quasi-static conditions pertinent for problems such as hydrocephalus, where the steady-state configuration is reached over a long period (more than a week).

Our analysis ignores material non-linearities of the solid matrix. Nevertheless, our results show that the model captures the dominant quantitative features of the disease. The calculations in this work offer a benchmark for numerical codes based on a more complete non-linear theory.

Subsequent work will address the absorption of the CSF through the venular bed of the brain as well as the transient problem of the progression

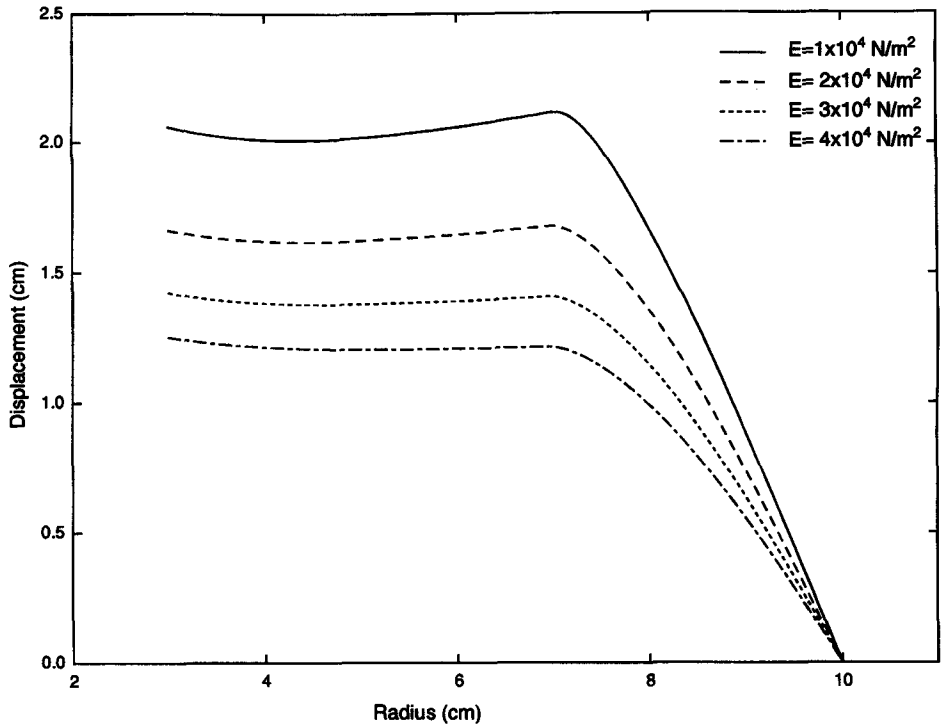

Figure 11. Radial displacement vs distance from ventricular surface for different elastic moduli.

of the disease with time. We are also engaged in finite-element calculations using actual geometries obtained from the computed tomographic scans of patients.

We acknowledge with thanks the many useful discussions we have had with Professor G. Tenti (University of Waterloo).

Appendix

Equilibrium Equations for Permeable Membrane. A cylindrical permeable membrane of circular cross-section is considered. On the outer surface, the membrane interacts mechanically with the adjoining porous matter (brain). The interior of the cylinder is filled with fluid. A constant amount of fluid flows through the membrane under the pressure difference on both sides of the membrane. The thickness of the membrane is assumed to be small enough in comparison with its radius, r^v, so that the stress inhomogeneity in the direction perpendicular to the surface may be neglected. A small element of the membrane defined by angle $d\phi$ (see Fig. A1) will be considered to find the equilibrium equation for the membrane matrix and the equation which governs the fluid flow. Since the macroscopic approach is adopted, the size of the membrane element $r^v\, d\phi$ has to be much larger than the characteristic size of the membrane pores. Considering the solid matrix and fluid individually, the condition for balance of forces for the element $d\phi$ in the direction defined by the

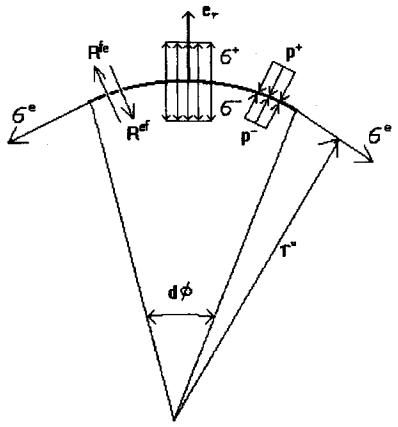

Figure A1. A small element of the membrane.

unit normal vector in the center of the element, $\mathbf{e}_r$, gives us

$$-2\sigma^e \sin\left(\frac{d\phi}{2}\right) + (\sigma^+ - \sigma^- + R^{fe})r^v\, d\phi = 0, \tag{A1}$$

$$[-(p^+ - p^-)n_e + R^{ef}]r^v\, d\phi = 0, \tag{A2}$$

where σ^e is the circumferential component of the membrane stress, σ^+ and σ^- are radial components of stress vectors acting on the outer and inner surface of the membrane matrix, p^+ and p^- are pore pressures given on the outer and inner surface of the membrane, and R^{fe} $(= -R^{ef})$ is the interaction force between fluid and membrane matrix. Since the equations (A1) and (A2) have to be valid for any small element of the membrane, and for small angles $d\phi$, $\sin(d\phi/2) \cong d\phi/2$, the equilibrium equation for the membrane matrix and fluid flow equation read as follows:

$$\sigma^e - (\sigma^+ - \sigma^- + R^{fe})r^v = 0, \tag{A3}$$

$$-(p^+ - p^-)n_e + R^{ef} = 0. \tag{A4}$$

Integration Constants. The constants C_2–C_4 are given for Cases I, II and III.

Case I.

$$C_1 = Qr^s, \qquad C_2 = \frac{\kappa}{B-C}(r^s)^{1-v_1} - V_0(r^s)^{v_2-v_1}, \qquad C_3 = V_0, \tag{A5}$$

$$C_4 = 1 + \frac{2\kappa M}{B-C}\ln r^s - M\left[\frac{\kappa}{B-C}(r^s)^{1-v_1} - V_0(r^s)^{v_2-v_1}\right]\frac{v_1+1}{v_1-1}(r^s)^{v_1-1}$$

$$- MV_0\frac{v_2+1}{v_2-1}(r^s)^{v_2-1} \tag{A6}$$

where

$$V_0 = \frac{[v_1(2\mu+\lambda)+\lambda](r^v)^{v_1-1}(r^s)^{1-v_1} - 2(\mu+\lambda)}{[v_1(2\mu+\lambda)+\lambda](r^v)^{v_1-1}(r^s)^{v_2-v_1} - [v_2(2\mu+\lambda)+\lambda](r^v)^{v_2-1}} \frac{\kappa}{B-C}. \tag{A7}$$

Case II.

$$C_1^w = C_1^q = Qr^s, \tag{A8}$$

$$C_1^w = \frac{1}{T_{22}}(T_{24} - V_1 T_{23}), \qquad C_2^g = \frac{1}{T_3}(T_5 + V_2 T_4), \tag{A9}$$

$$C_3^w = V_1, \qquad C_3^g = V_2, \tag{A10}$$

$$C_4^w = \frac{T_{23}T_6 - T_7T_{22}}{T_{23}T_{16} - T_{17}T_{22}}\left[\frac{T_{16}T_{24}}{T_{22}} - T_{18} - \frac{T_{19}T_5}{T_3} + T_{21} + V_2\left(\frac{T_{19}T_4}{T_3} - T_{20}\right)\right]$$
$$- V_2\left[\frac{T_4(T_8 - T_1)}{T_3} - T_9 + T_2\right] - \frac{T_{24}T_6}{T_{22}} + \frac{T_5(T_8 - T_1)}{T_3}, \tag{A11}$$

$$C_4^g = -\frac{1}{T_3}(T_5 - V_2T_4)T_1 - V_2T_2, \tag{A12}$$

where

$$V_1 = \frac{T_{22}}{T_{23}T_{16} - T_{17}T_{22}}\left[V_2\left[\frac{T_4(T_8 - T_1)}{T_4} - T_9 - T_2\right] + \frac{T_{16}T_{24}}{T_{22}} - \frac{T_{19}T_5}{T_3} - T_{18} + T_{21}\right], \tag{A13}$$

$$V_2 = \frac{\left(\frac{T_{10}T_{24}}{T_{22}} - \frac{T_{13}T_5}{T_3} - T_{12} + T_{15}\right)\left(\frac{T_{23}T_{16}}{T_{22}} - T_{17}\right) - \left(\frac{T_{16}T_{24}}{T_{22}} - \frac{T_{19}T_5}{T_3} - T_{18} + T_{21}\right)\left(\frac{T_{23}T_{10}}{T_{22}} - T_{12}\right)}{\left(\frac{T_{19}T_4}{T_3} - T_{20}\right)\left(\frac{T_{23}T_{10}}{T_{22}} - T_{11}\right) - \left(\frac{T_{23}T_{16}}{T_{22}} - T_{17}\right)\left(\frac{T_4T_{13}}{T_3} - T_{14}\right)}, \tag{A14}$$

$$T_1 = \frac{M^gQr^s\mu^f(v_1^g+1)}{k_0^g(v_1^g-1)}(r^s)^{v_1^g-1}, \qquad T_2 = \frac{M^gQr^s\mu^f(v_2^g+1)}{k_0^g(v_2^g-1)}(r^s)^{v_2^g-1}, \tag{A15}$$

$$T_3 = (r^s)^{v_1^g}, \qquad T_4 = (r^s)^{v_2^g}, \qquad T_5 = -\frac{r^s}{2M^g}, \tag{A16}$$

$$T_6 = \frac{M^wQr^s\mu^f(v_1^w+1)}{i_0^w(v_1^w-1)}(r^i)^{v_1^w-1}, \qquad T_7 = \frac{M^wQr^s\mu^f(v_2^w+1)}{k_0^w(v_2^w-1)}(r^i)^{v_2^w-1}, \tag{A17}$$

$$T_8 = \frac{M^gQr^s\mu^f(v_1^g+1)}{k_0^g(v_1^g-1)}(r^i)^{v_1^g-1}, \qquad T_9 = \frac{M^gQr^s\mu^f(v_2^g+1)}{k_0^g(v_2^g-1)}(r^i)^{v_2^g-1}, \tag{A18}$$

$$T_{10} = (r^i)^{v_1^w}, \qquad T_{11} = (r^i)^{v_2^w}, \qquad T_{12} = -\frac{r^i}{2M^w}, \tag{A19}$$

$$T_{13} = (r^i)^{v_2^g}, \qquad T_{14} = (r^i)^{v_2^g}, \qquad T_{15} = -\frac{r^i}{2M^g}, \tag{A20}$$

$$T_{16} = [(2\mu^w + \lambda^w)v_1^w + \lambda^w](r^i)^{v_1^w - 1}, \qquad T_{17} = [(2\mu^w + \lambda^w)v_2^w + \lambda^w](r^i)^{v_2^w - 1}, \tag{A21}$$

$$T_{18} = -\frac{\mu^w + \lambda^w}{M^w}, \qquad T_{19} = [(2\mu^g + \lambda^g)v_1^g + \lambda^g](r^i)^{v_1^g - 1}, \tag{A22}$$

$$T_{20} = [(2\mu^g + \lambda^g)v_2^g + \lambda^g](r^i)^{v_2^g - 1}, \qquad T_{21} = -\frac{\mu^g + \lambda^g}{M^g}, \tag{A23}$$

$$T_{22} = [(2\mu^w + \lambda^w)v_1^w + \lambda^w](r^v)^{v_1^w - 1},$$

$$T_{23} = [(2\mu^w + \lambda^w)v_2^w + \lambda^w](r^v)^{v_2^w - 1}, \qquad T_{24} = -\frac{\mu^w + \lambda^w}{M^w}, \tag{A24}$$

and v_i^m ($i = 1, 2$, and $m = w, g$) are roots of the equation

$$(v^m)^2 - \frac{\mu^f M^m Q r^s}{(2\mu^m + \lambda^m)k_0^m} v^m - 1 - \frac{\mu^f M^m Q r^s}{(2\mu^m + \lambda^m)k_0^m} = 0. \tag{A25}$$

Case III. The integration constants C_1^m–C_4^m ($m = w$ and g) and parameters T_1–T_{21} are defined exactly as for case II, while parameters T_{22}, T_{23} and T_{24} read

$$T_{22} = \left[\frac{\alpha_e}{r^v} + \frac{\mu^f M^e Q r^s}{k_{e0} r^v} - [(2\mu^w + \lambda^w)v_1^w + \lambda^w]\right](r^v)^{v_1^w - 1}, \tag{A26}$$

$$T_{23} = \left[\frac{\alpha_e}{r^v} + \frac{\mu^f M^e Q r^s}{k_{e0} r^v} - [(2\mu^w + \lambda^w)v_2^w + \lambda^w]\right](r^v)^{v_2^w - 1}, \tag{A27}$$

$$T_{24} = \frac{\mu^f Q r^s}{k_{e0} r^v} - \frac{1}{2M^w}\left[\frac{\alpha_e}{r^v} + \frac{\mu^f M^e Q r^s}{k_{e0} r^v} - 2(\mu^w + \lambda^w)\right]. \tag{A28}$$

On Definition of Poisson's Ratio in Two-Phase Model of Brain Matter. The Poisson's ratio, ν is defined as the ratio between the lateral contraction (the induced lateral strain) of solid specimen and the elongation in the direction of the applied strain. This definition is unique for homogeneous materials, for which the Poisson's ratio depends only on the properties of the materials, and in the isotropic case, ν assumes values between -1 and 0.5 (Fung, 1994). The upper limit refers to incompressible media.

For inhomogeneous, multi-phasic materials like brain tissue, the Poisson's ratio depends not only on the properties of materials but also on the definition of strain and, in certain cases, on conditions the material is subjected to during the test. The dependence of ν on the definition of strain results from the fact that the strain measures for inhomogeneous materials may refer either to the mixture as a whole or to particular phases of the material (Kaczmarek, 1992). Another important factor which determines the Poisson's ratio of saturated porous materials is whether the drained or undrained test is performed (this refers respectively to whether flow of fluid through the outer surface of the sample is allowed or not). As a result, two independent Poisson's ratios, ν and ν_u, corresponding to drained and undrained conditions, may be defined for isotropic porous materials: $\nu = (3K - 2G)/[2(3K$

$+ G)]$, and $\nu_u = (3K_u - 2G)/[2(3K_u + G)]$, where K and K_u are the drained and undrained bulk moduli, and G is the shear modulus which is usually assumed to be identical for drained and undrained conditions. The upper limit for ν_u, equal to 0.5, corresponds to phases incompressible on the microscopic level. For isotropic materials, the lateral response of the porous material to a given longitudinal strain is always larger for undrained than for drained conditions. Thus we have (Kumpel, 1991)

$$\nu < \nu_u \leq 0.5. \tag{A29}$$

It is assumed in this paper that the relative motion of the fluid with respect to the solid skeleton is significant and that the materials of phases are incompressible. As a result, the parameters which enter the effective stress law, given by equation (9), are related to the drained Poisson's ratio. To our knowledge, the differences between values of ν and ν_u for brain matter have not been studied. The data for soft geological materials, however, show that ν becomes significantly smaller than ν_u (Detournay, 1993).

It should be noted that the above definitions of the Poisson's ratio refer to steady or quasi-steady state of materials. This presumes that the time between measurements of initial and final state of deformation is much larger than the time needed for escape of fluid from the loaded drained porous material, and then the characteristic relaxation time for the matrix deformation itself. Such conditions are probably not satisfied during experiments such as that of Metz *et al.* (1970), the results of which have been used to obtain the values for the parameters in Table 1.

REFERENCES

Atkin, R. J. and R. E. Craine. 1976. Continuum theories of mixtures: applications. *J. Inst. Math. Appl.* **17**, 153.

Biot, M. A. 1941. General theory of three-dimensional consolidation. *J. Appl. Phys.* **12**, 155.

Bowen, R. M. 1976. Theory of mixtures. In *Continuum Physics*, A. C. Eringen (Ed), Vol. II. New York: Academic.

Detournay, E. 1993. Fundamentals of poroelasticity. In *Comprehensive Rock Engineering: Principles, Practice, and Projects*, C. Fairhurst (Ed). Elmsford, NY: Pergamon.

Drake, J. M., O. Mostachfi, G. Tenti and S. Sivaloganathan. 1996. Realistic simple mathematical model of brain biomechanics for computer simulation of hydrocephalus and other brain abnormalities. *Can. J. Neurol. Sci.* **23**, S5 (abstract).

Fung, Y. C. 1994. *A First Course in Continuum Mechanics for Physical Scientists and Engineers*. Englewood Cliffs, NJ: Prentice-Hall.

Hakim, S. and C. Hakim. 1984. A biomechanical model of hydrocephalus and its relationship to treatment. In *Hydrocephalus*, K. Shapiro and A. Marmarou (Eds). New York: Raven.

Hirano, A. 1993. Edema and myelin-associated extracellular spaces. In *Brain Edema*, Y. Inaba, I. Klatzo and M. Spatz (Eds). Berlin: Springer-Verlag.

Jayaraman, G. 1983. Water transport in the arterial wall—a theoretical study. *J. Biomech.* **16**, 833.

Kaczmarek, M. 1992. On kinematics in the theory of multiphase media, comparison between two traditions. *Mech. Res. Comm.* **19**, 361.

Kenyon, D. E. 1976. Transient filtration in porous elastic cylinder. *J. Appl. Mech.* **43**, 594.

Klanchar, M. and J. M. Tarbell. 1987. Modeling water flow through arterial tissue. *Bull. Math. Biol.* **49**.

Kumpel, H.-J. 1991. Poroelasticity: parameters reviewed. *Geophys. J. Int.* **105**, 783.

Lux, W. E., G. M. Hochwald, A. Sahar and J. Ransohoff. 1970. Periventricular water content. *Arch. Neurol.* **23**, 475.

Metz, H., J. McElhaney and A. K. Ommaya. 1970. A comparison of the elasticity of live, dead and fixed brain tissue. *J. Biomech.* **3**, 453.

Mow, V. C., S. C. Kuei, W. M. Lai and C. G. Armstrong. 1980. Biphasic creep and stress relaxation of articular cartilage: theory and experiments. *J. Biomech. Eng.* **102**, 73.

Nag, S. 1991. In *Textbook of Neuropathology*, R. L. Davis and D. M. Robertson (Eds), p. 95. Baltimore: William and Wilkins.

Nagashima, T., B. Horwitz and S. I. Rapoport. 1990. A mathematical model for vasogenic brain edema. *Adv. Neurol.* **52**, 317.

Nagashima, T., N. Tanaki, S. Matsumoto, B. Horwitz and Y. Seguchi. 1987. Biomechanics of hydrocephalus: a new theoretical model. *Neurosurgery* **21**, 898.

Nyberg-Hansen, R., A. Tovik and R. Bhatia. 1975. On the pathology of experimental hydrocephalus. *Brain Res.* **95**, 343.

Oloyede, A. and N. D. Broom. 1991. Is classical consolidation theory applicable to articular cartilage deformation? *Clin. Biomech.* **6**, 206.

Pasquini, U., M. Bronzini, E. Gozzoli, P. Mancini, F. Menichelli and U. Salvolini. 1977. Periventricular hypodensity in hydrocephalus: a clinico-radiological and mathematical analysis using computed tomography. *J. Comp. Assist. Tomography* **1**, 443.

Rabenstain, A. L. 1972. *Introduction to Ordinary Differential Equations*. New York: Academic.

Rall, D. P., W. W. Oppelt and C. S. Patlak. 1962. Increased extracellular space of brain as determined by diffusion of inulin from the ventricular system. *Life Sci.* **1**, 43.

Rekate, H. and W. Olivero. 1990. *Hydrocephalus*, R. M. Scott (Ed), p. 11. Baltimore: William and Wilkins.

Reulen, H. J., R. Graham, M. Spatz and I. Klatzo. 1977. Role of pressure gradients and bulk flow in dynamics of vasogenic brain edema. *J. Neurosurgery* **46**, 24.

Subramaniam, R. P., S. R. Neff and R. Pakal. 1995. A numerical study of the biomechanics of structural neurologic diseases. In *High Performance Computing 1995—Grand Challenges in Computer Simulation*, A. Tentner (Ed), p. 552. San Diego: Society for Computer Simulation.

Weller, R. O. and J. Mitchell. 1980. Cerebrospinal fluid edema and its sequelae in hydrocephalus. *Adv. Neurol.* **28**, 111.

Yang, M. and L. A. Taber. 1991. The possible role of poroelasticity in the apparent viscoelastic behavior of cardiac muscle. *J. Biomech.* **24**, 587.

Received 14 November 1995
Revised version accepted 18 July 1996